A Galvanic Isolated Amplifier based on CMOS Integrated Hall-effect Sensors

Seyed Sepehr Mirfakhraei[1], Yves Audet[1], Ahmad Hassan[1], and Mohamad Sawan[1,2]
[1]Polystim Neurotech Lab., Electrical Engineering Department, Polytechnique Montréal, Montréal, Canada
[2]CenBRAIN, School of Engineering, Westlake University, and Westlake Institute of Advanced Sciences, Hangzhou, Zhejiang, China
seyed-sepehr.mirfakhraei@polymtl.ca

***Abstract*— A novel galvanic isolated amplifier based on CMOS integrated Hall sensors is presented in this paper. Two serially connected Hall-effect sensors are integrated along with their instrumentation amplifiers using the TSMC 65nm process. A printed-circuit board is employed to validate the proposed isolation amplifier by assembling the chip with chopper modulator, coil driver, miniature coil, variable gain amplifier, and anti-aliasing filter. Because of the miniaturized size of isolation components, this approach can be packaged in chip for industrial applications. This solution replaces the need of bulky/frequency dependent current transformers, complex isolation amplifiers with embedded analog to digital converters, and allows proposed sensors to be used in voltage and current sensing applications. The introduced prototype achieves an input referred offset of 1 mV, 50 dB full-scale signal-to-noise ratio in a 10 kHz bandwidth, and spurious-free dynamic range of 53 dB, while satisfying continuous isolation working voltage of 550 V.**

***Index Terms*— Isolated amplifier, current/voltage sensing, galvanic isolation, chopper amplifier, magnetic coil, CMOS Hall sensor.**

I. Introduction

POWER monitoring applications such as power system control and protection need to simultaneously measure the load voltage and current. Such devices must continuously withstand in their working High Voltage (HV) environment for their lifetime and tolerate one-minute operation in presence of lightning surges, faults, or switching loads [1]. Additionally, they must have a fast response time to react to any aggression. Consequently, stringent industrial standards [1] verify their reliability over the required lifetime as well as satisfying important electrical safety features.

The principal technique employed in isolation/galvanic amplifiers (GA) is segregated ground loops and dividing the amplifiers into an HV side and a Low Voltage (LV) side. Therefore, the sensed voltage and current by the HV side must be transmitted to the LV side through an isolation medium. Fig. 1 summarizes all available isolated voltage/current sensing techniques. Unlike current transformers (CT) and magnetic sensors including Hall sensor, giant magneto resistor (GMR), and anisotropic magneto resistors (AMR) which are restricted to current sensing, implementation of differential voltage amplifiers is not limited to voltage sensing and are extensively used in shunt resistor current sensing due to the shunt simple implementation and high frequency behavior.

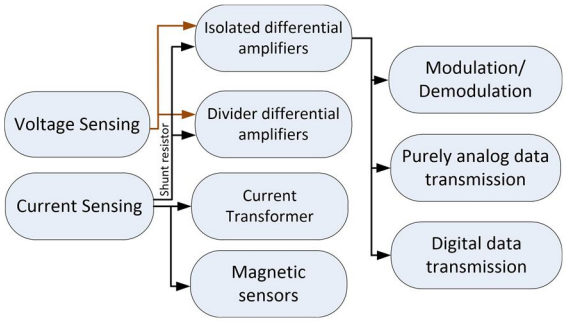

Fig. 1. Available isolated voltage and current sensing.

In isolated differential amplifiers, data transmission is performed by modulation, digitization, or purely analog. Commonly used isolated media are capacitive [2], inductive [3], and optic [4]. Purely analog data transmission is a challenge for capacitive link, as it transmits the HV side's common mode noises ranging from 50 Hz to 400 Hz (supply noise) to 1.5 kHz (lightning strike noise) [5]. Hence, modulation and demodulation are performed to separate the signal from the common mode noise, and the LV side high pass filter rejects the common mode transient noise as in Fig. 2(a). So far, pulse width modulation (PWM) [6] and amplitude modulation (AM) [7] are employed in modulation/ demodulation types of GA. The PWM induces residual clock noise on the output signal. Also, in inductive medium, achieving a good Signal to Noise Ratio "SNR" imposes designers to employ a high-quality factor transformer which is not possible in millimeter scale, and lead to an enlarged overall design [7].

In parallel, the robust performance of digital isolators allows designers to use all types of isolation barriers as shown in Fig. 2(b), to overcome the previous limitations, and keep a high signal-to-noise ratio (SNR) [2, 3]. However, in addition to the transceiver and the receiver of the digital isolator, it comes at the cost of an additional analog-to-digital converter (ADC) on the HV side and a digital-to-analog converter (DAC) on the LV side. Despite the compactness and significant performance

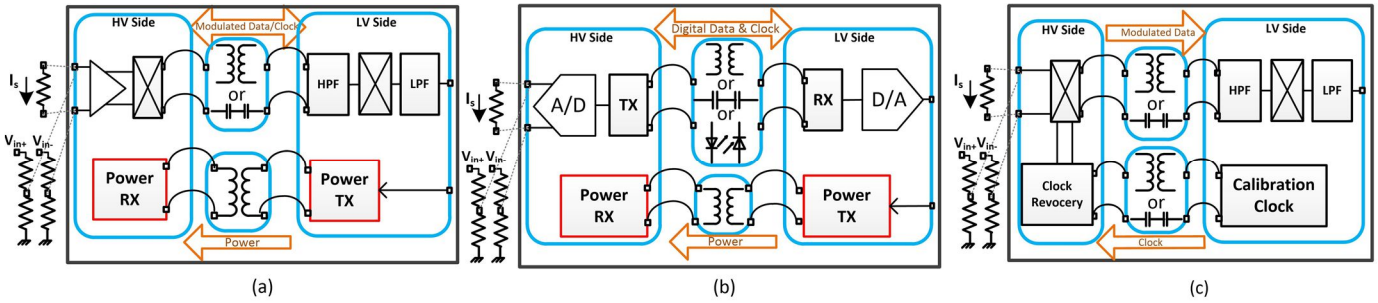

Fig. 2. Isolation Amplifier based on Modulation/Demodulation (a) with active circuitry on the HV side, (b) based on digital isolator, and (c) all passive components on the HV side.

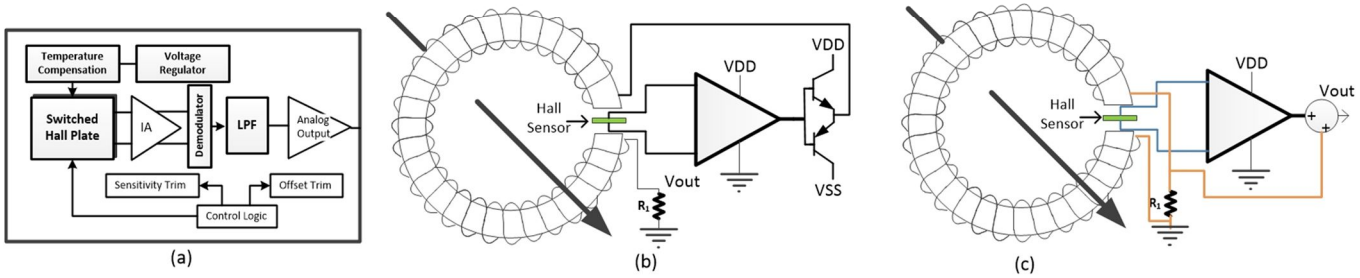

Fig. 3. Isolated current sensing: (a) internal architecture of a typical Hall amplifier, (b) Hall current sensing using magnetic concentrator in closed loop configuration, and (c) combination of CT and Hall sensors for wide bandwidth current measurement.

characteristics, the overall design is complicated and precise synchronization between ADC's sampling time and rectifier is needed.

In fully isolated or single supply isolation amplifiers, the power of HV side is supplied by the LV side as shown in Fig. 2(a-b). Therefore, the power consumption of the HV side will be the dominant part of the overall system's consumption. As shown in Fig. 2(c), in modulator/demodulator type, there are attempts to not use active components on the HV side, such that chopper switches are triggered by a passive recovery clock [8, 9]. However, the transformer-based GA is limited to current sensing [8], and the capacitive based GA has a limited resolution which makes it not suitable for high resolution applications [9]. The other drawback of all fully isolated amplifiers using digital communication is having high-power consumption on their HV side. For instance, the power consumption of one ADC on the HV side can is around 100 mW [3].

Analog data transmission with optocouplers is an attractive alternative that can reach a very good linearity of 0.1% and high isolation level of 5 kVrms [10]. However, they suffer from light-emitting diode (LED) shorter lifetime being caused by electrical and thermal stresses [11]; displacement damage subject to gamma radiation, also lowers the quantum efficiency of the optocouplers [12]. Other types of differential amplifiers that can tolerate HV conditions are resistor divider and capacitive coupling that are mostly used in biopotential amplifiers. However, both have not been discussed here because of not being truly isolated and DC blockage of signal, respectively.

In CT-based solution, AC current in the primary of the HV side is transformed to a smaller current on its secondary winding and converted to voltage using a burden resistor. Not capable of DC transmittance, this approach also suffers from bulky transformers for low-frequency signals [13].

While there have been limited efforts to configure Hall effects as voltage amplifiers [14, 15], they have been widely used in current and position sensors, magnetic field, and speed measurements [16]. High DC offset, 1/f noise, offset and sensitivity drift over temperature are of the concerns in deploying Hall sensors [14]. Consequently, every Hall current sensor amplifier integrates a Hall element, temperature-compensating circuitry, a small-signal high-gain amplifier, a clamped low-impedance output stage, and a proprietary dynamic offset cancellation technique as shown in Fig. 3(a) [17].

Typical CMOS Hall sensors are known for their low sensitivity. As a result, traditionally large C-shaped magnetic concentrator being clamped around wires, as shown in Fig. 3(b), is usually used [13]. In this configuration, the signal of the magnetic sensor generates a current signal opposing the offset magnetic field, and the remaining current will generate the signal related current to produce the output voltage on R_1. However, the low bandwidth of the core material due to eddy losses and hysteresis, decreases the overall sensor's frequency response. To overcome the bandwidth limit, Fig. 3(c) combines the output of open-loop magnetic sensor and a CT to achieve wide bandwidth current measurement [13]. Although the Hall current sensor with concentrator demonstrates good resolution, linearity, and bandwidth, the final product is bulky in comparison with the traditional analog isolation amplifier. There are state-of-the-art and industrial Hall sensors that the sensor is placed on top of a shunt of current [18, 19] or a high current are diverted into the package [17, 20] and the magnetic field created by this high current is being sensed. However, their usage is limited for high current applications, and yet, similar to all the magnetic sensors, they are limited to current sensing.

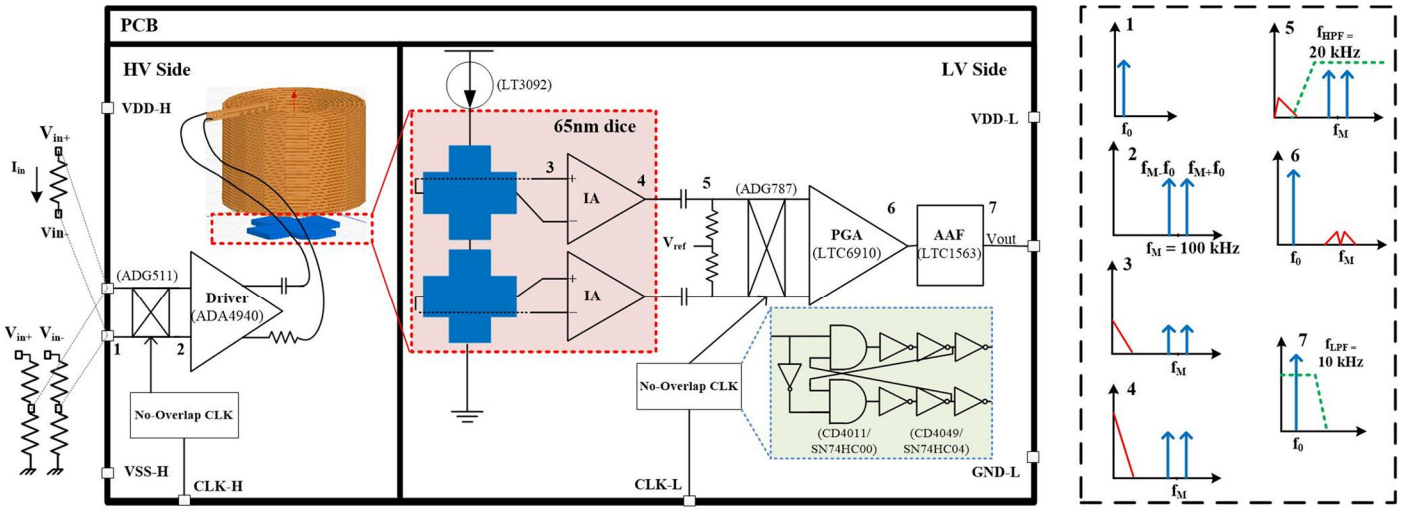

(a) (b)

Fig. 4. (a) Architecture of the Hall based isolated amplifier, and (b) signal spectrum at various stages of the amplifier.

Our response to these challenges is a Hall-based isolation amplifier capable of sensing shunt resistor voltage on the high voltage lines as well as differential voltage sensing. In this approach, the HV side is directly connected to the shunt resistor or differential voltage lines and generates a perpendicular signal dependent magnetic field to be sensed by the Hall sensors on the LV side. Consequently, it enables the Hall sensor to be utilized in voltage sensing applications, and the magnetic data transmission adds a galvanic medium to satisfy requisite isolation. Also, the analog-based approach eliminates the complications involved in using ADCs on the HV side and consequently conserve the overall system's power consumption.

The capacitive data transmission of Fig. 2 (a & c) transmits electrical surges that has inherently low frequencies. To protect the amplifier from surges, the modulation/demodulation approach, as well as high pass filtering at the LV side, are performed. Although the isolation principle of an inductive link is realized by magnetic coupling, yet the planner inductors behave like parallel capacitor plates and they suffer from surge transmission as well. Moreover, the modulation/demodulation approach comes with the benefit of lowering the transformer size in inductive coupling technique; nonetheless, limitation of the quality factor in small planner coils made the amplifier bulkier and power-hungry [7]. Also, inductive links are sensitive to electromagnetic interference [21]. Consequently, most of the integrated inductive links are used as digital isolators [3]. The purely magnetic-based approach of the Hall based isolation amplifier not only immunes the amplifier to surges but also require a smaller footprint transmitter coils with the advantage of generating more magnetic field with lower inductance while preserving consumption.

The remaining of this paper is organized as follows: the overall system architecture is described in Section II, coil, and sensor design criteria, and implementation of the instrumentation amplifier (IA) are also, described in this section. The measurement results and discussion are stated in Section III, and finally conclusion remarks and future works appear in Section IV.

II. Design and Implementation

A. Overview

The main architectural concerns of the proposed Hall based isolation amplifiers are a miniature coil with its driver, the twin CMOS Hall effect sensors with their respective IAs, and the Anti-Aliasing Filter (AAF). A schematic version of the Hall based isolation amplifier is shown in Fig. 4 (a).

First, located on the HV side, chopper modulator displaces the input signal to a higher frequency band of 100 kHz. Second, a variable gain amplifier drives the miniature coil being placed on top of two serried CMOS Hall sensors with their respective IAs fabricated in 65nm chip. Consequently, the coil generates a signal dependent magnetic field to be sensed by the sensors and amplified by the integrated IAs. Then, implemented on the PCB, a passive high pass filter (HPF) with a cutoff frequency of 20 kHz eliminates the DC offset and attenuates the 1/f noise of the combined sensors and IAs. Next, down converter chopper switches bring the signal back to the baseband region, and a programmable gain amplifier further adjusts the gain. Finally, the mirrored spectral components due to switching frequency and residual switching glitches are being filtered by an active low pass AAF.

The frequency spectrum of the GA is shown in Fig. 4 (b). The modulation/demodulation technique in graph 2 and 6 of Fig. 4 (b) allows transmission of baseband input with signal's DC component to the Hall sensor without letting flicker noise as well as DC offset of the sensor and IA being merged with the received signal.

In comparison with similar works, at [14] CMOS Magfets are used as the sensing element which eliminates the need for instrumentation amplifiers and a cascode stage amplifies the deflected current due to magnetic field; however, minimum detectable magnetic field in CMOS Magfets is higher than CMOS Hall sensors [22]. Therefore, by using CMOS Hall sensors better detection of the magnetic field will be achieved.

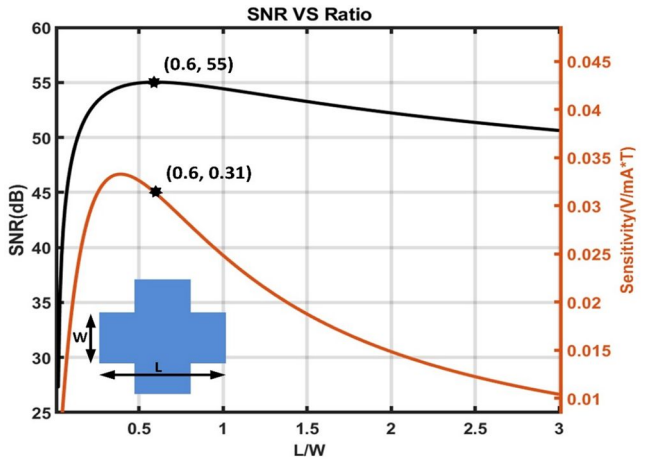

Fig. 5. Calculated sensor's SNR and Sensitivity respective with L/W (1 mA biasing current and 2.5 mT of magnetic field).

TABLE I
MODEL PARAMETERS BASED ON THE AVAILABLE TECHNOLOGY AND FIELD STRENGTH OF THE MINIATURE COIL

Symbol	PARAMETER	Value
n [cm^{-3}]	Dopping Concentration	$2e^{17}$
I [mA]	Biasing Current	1
B [mT]	Peak Magnetic field of miniature coil	2.6
R_s	N-Well Sheet Resistance	1e3
t [µm]	N-Well Thickness	1
σ [$\frac{S}{m}$]	Conductivity	$\frac{1}{R_S \times t}$
μ_H	Hall Mobility	$\frac{\sigma}{n \times q}$

Also, the structure presented in [15], allows single magnetic link to transfer analog data and no additional data link for clock recovery is needed; however, an external low-frequency magnetic field can perturb the amplifier's signal, and the modulation/ demodulation approach not only protects the amplifier from such noises, but also removes the necessity of an active offset canceler circuit.

B. Sensor Implementation

CMOS Hall sensors are known for low sensitivity. Therefore, optimum sizing to achieve the highest SNR is performed as following. The Hall voltage related sensitivity is defined by:

$$S_V = \frac{G \times \mu_H}{N_{square}} \tag{1}$$

$$G = 1 - 1.045e^{-\pi \times \frac{L}{W}} \tag{2}$$

where G is the geometry parameter [23], μ_H the Hall mobility, N_{square} the equivalent square number of N-Well sheet resistance, L the length, and W the width of the sensor. Knowing the sensitivity, the sensor's biasing current, I, and the peak magnetic field of the coil, B, the peak voltage of the sensor is calculated as:

$$V_{peak} = S_V \times I \times B \tag{3}$$

To determine the noise power, flicker noise, as well as DC offset, is ignored due to the modulation technique. Also, value of shot noise of the tail current source is negligible and can be

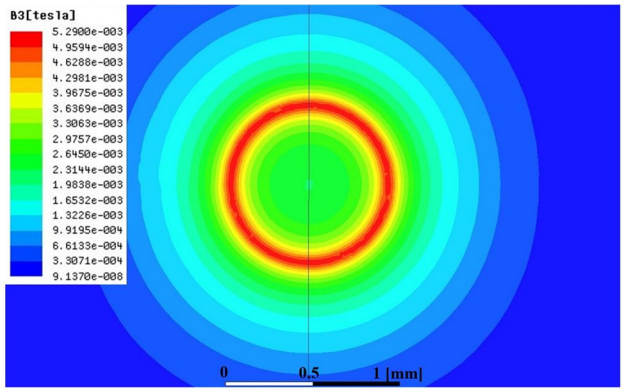

Fig. 6. Simulated radial magnetic field at 17.5 µm distance from the bottom of the miniature coil with 2.5 mA of current.

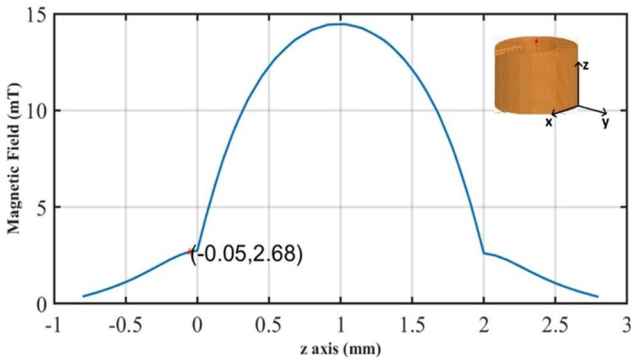

Fig. 7. Simulation result of axial magnetic field of the miniature coil with 2.5 mA of current.

further attenuated by the amplifier's CMRR. Therefore, the main noise contributor on the output nodes of the sensor is thermal noise which is calculated as:

$$Noise = \sqrt{4kTR_{eq}} \tag{4}$$

$$R_{eq} = (2\frac{L}{W} + \frac{2}{3})R_s \tag{5}$$

where R_{eq} is the equivalent resistor between voltage nodes of the sensor [23]. As shown in Fig. 5, $\frac{L}{W}$ ratio of 0.58 results in the optimum SNR. Hence, the implemented sensor has 7.2 µm width and length of 12 µm. To reduce the 1/f noise and carrier surface loss, the sensor's top is covered with P^+ layer [24]. Table I summarizes the parameters used in the calculation which corresponds to the available technology and test setup.

C. Miniature Coil

System's overall SNR is directly related to the strength of the magnetic field generated by the HV side's driver. Unlike the previous studies, in this work, the coil current is supplied by the HV side's driver; thus, to restrict the power consumption and maintain good SNR, a limited current should be fed to the coil for high magnetic field generation. On the other hand, the coil size must be minimized to make this design compatible with IC packaging, and miniaturization is another challenge that cannot be done using conventional concentrators.

One viable solution to have a compact design is using miniature coils. For such a reason, a small air gap solenoid coil

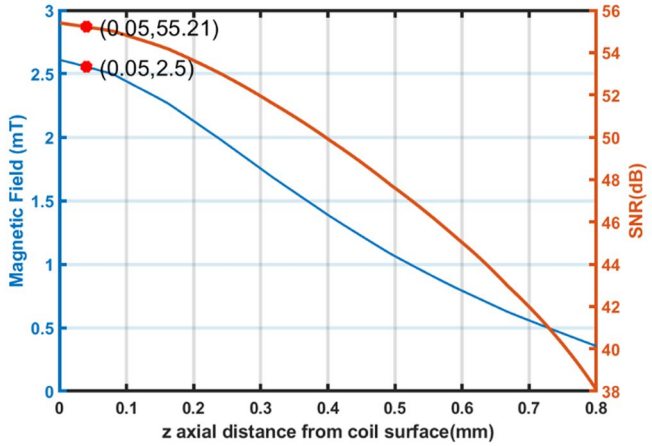

Fig. 8. Variation of SNR and magnetic field respective with axial separation of the chip substrate where coil is located at the chip's surface.

TABLE II
EXTERNAL MINIATURE COIL PARAMETERS

	PARAMETER	Value
Miniature coil	Inner diameter	1 mm
	Outer diameter	1.9 mm
	Height	1.9 mm
	Turns	270
	Wire width without isolator	50 µm
	Wire width with isolator	69µm
	Coating	Polyamide
	Enamel thickness	~10µm
	Wire type	AWG44-HY
Ferrite	Material	78
	Outer diameter	1mm
	Initial permeability	2000
	Relative permeability	48

is manufactured and to further increase magnetic field, a ferrite rod is centered at the coil's airgap. The coil will be placed directly on the sensor dice. Therefore, assuming zero gap between the coil and sensor die, the actual distance between the die's N-Well top and the coil's wire surface will be the sum of a 9.5 µm of coil isolator material plus 10 µm of dice intermetal isolation.

Fig. 6 shows the magnetic field simulation of the described miniature coil using ANSYS Maxwell software at 17.5 µm distance from the coil. The coil generates a uniform peak magnetic field of 2.5 mT at the center for 2.5 mA of current. This allows the twin sensors to absorb identical magnetic field. The field strength relative to the coil's height is also shown in Fig. 7. Because of the complications involved in placing the dice in the coil center, the highest field of the coil cannot be captured, and we can only place the sensor on the coil's edges. The coil-ferrite specification is described in Table II. Using the optimum sensitivity of Fig. 5 and simulated axial magnetic field of Fig. 7, Fig. 8 demonstrates the relationship between SNR and magnetic field respective to axial distance. Although capturing the most magnetic field and achieving the optimum SNR stems from minimizing the coil-sensor distance, in applications with higher requirment of isolation level, adding layers of polyamid with 30 µm of thickness similar to [3] can increase the isolation

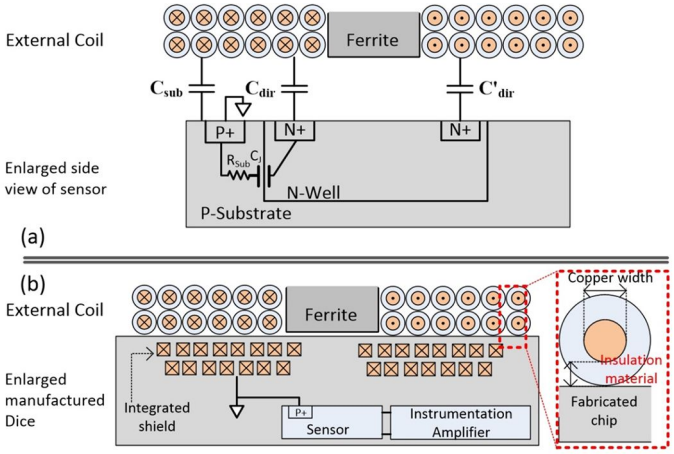

Fig. 9. Coil placement: (a) side view of the miniature coil-sensor with the respective parasitic, and (b) side view of the miniature coil and shielded sensor.

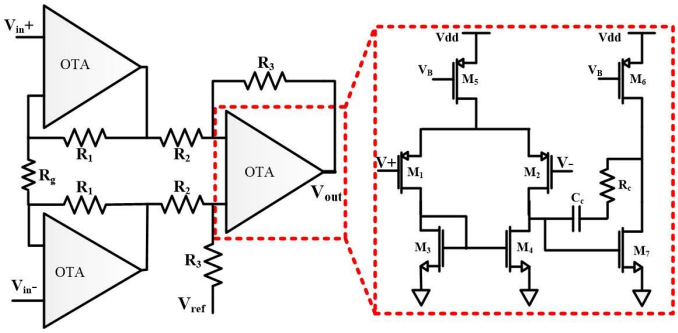

Fig. 10. Topology of the integrated instrumentation amplifier.

voltage while loosing only 0.5 dB.

D. Driver Circuit

To preserve the overall system's linearity, the current passing the miniature coil must be linearly proportional to the input voltage. Considering the coil as a simple series model of relatively large inductance and low resistance, frequency response of the model would have a pole lower than the chopper frequency. This causes non-flat low pass response of the overall system. Moreover, offset of the driver injects a constant DC current to the coil that not only can saturate the coil, but also generates a DC field that would be sensed by the sensor.

Therefore, as shown on the HV side of Fig. 4(a), using inductance of the miniature coil, a series RLC filter was created to ensure flat passband response and avoid a constant DC current injection through the coil. In this way, the maximum delivered current is also controlled. Finally, the gain of this stage must be tuned to adjust the deliverable coil's current for different input voltage ranges of shunt resistor current sensing or differential voltage sensing, so that maximum plausible magnetic field is delivered to the sensors in both sensing applications.

E. Instrumentation Amplifier Design

Coil placement on the sensor's top creates two type of parasitic capacitance. C_{dir} is capacitance between the coil and the integrated Hall sensor's metallic contacts and N-Well and C_{sub} is parasitic between coil and dice substrate which both are shown in Fig. 9(a). This parasitic effect exhibits two types of

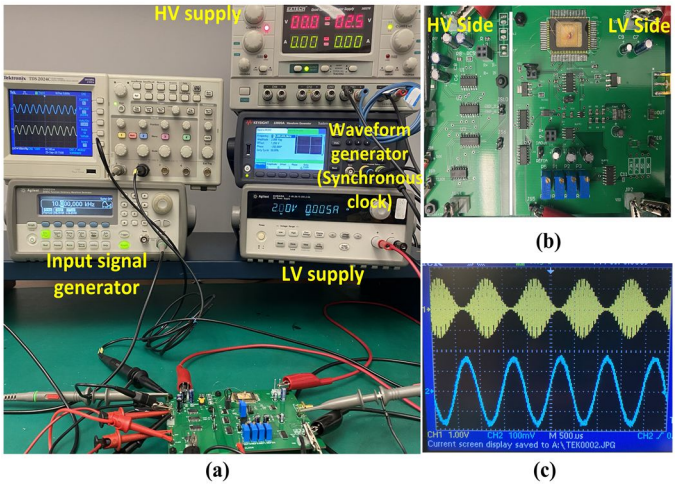

Fig. 11. Experimental measurement: (a) test bench setup, (b) prototype PCB of the design, and (c) modulated current of the miniature coil measured from the 2 kΩ resistor of the high voltage side's RLC network.

noises, common and differential mode [25], so the sensor's output signal will be defined as the following:

$$V_{out} = V_{CM} + V_{diff-CC} + V_H \quad (6)$$

where, V_{CM} is common mode noise, $V_{diff-CC}$ is capacitively coupled differential voltage noise, and V_H is the Hall voltage generated by the magnetic field. Using eq (3), reported data of Table (I), and sensor's sensitivity of Fig. 5, the sensor alone can induce a differential voltage of up to 75µV. Due to the small value of the input signal, damping and controlling the V_{CM} and $V_{diff-CC}$ are of great importance.

A typical approach in damping the V_{CM} of the CMOS Hall sensors is the placement of an instrumentation amplifier with a high Common Mode Rejection Ration (CMRR). Furthermore, as the Hall sensor does not have any driving capabilities, any capacitance on their signal node decreases their bandwidth [26]. Hence, an amplifier with high input impedance and no implemented input capacitance need to be employed. For this reason, here a conventional IA with the architecture shown in Fig. 10 has a CMRR of 90dB, 60 dB of gain, an input referred noise of 14 $\frac{nV}{\sqrt{Hz}}$, a cutoff frequency of 200 kHz, and gain-BW of 200 MHz is designed.

The $V_{diff-CC}$ is related to an asymmetry between the miniature coil and the Hall sensor as well as its connection. Such an inevitable asymmetry varies the C_{dir} parasitics which impose two distinct voltages on the sensor's nods in Fig. 9(a). Addressing the $V_{diff-CC}$ is done by a proper layout. Accordingly, the instrumentation amplifier is placed at a close distance to the sensor, while the Hall signals' wire lengths are precisely matched. The other countermeasure considered for this noise is creating an integrated shield surrounding the sensors and partially the IA. The grounded shield creates a uni-potential plate that shields the sensor from the noises generated by mismatched capacitors between the external coil and sensor Fig. 9(b). The entire substrate that surrounds the N-Well perimeter of the sensor is also tied to the ground to minimize the variation in C_{sub}.

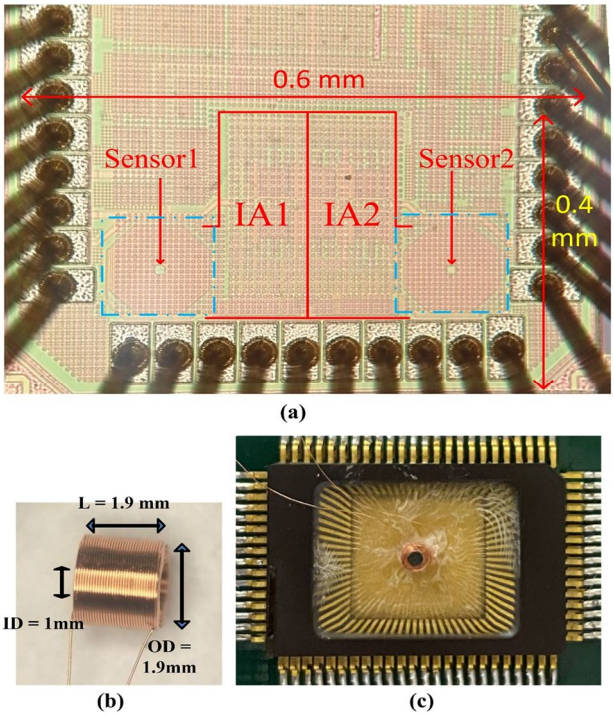

Fig. 12 System in package view: (a) micrograph of the manufactured sensors and instrumentation amplifiers, (b) manufacture miniature coil, and (c) sensor package with coil glued on top of the dice.

III. Measurement Results

A Hall based isolation amplifier is designed for voltage and current sensing using shunt resistors. The test bench setup and its dedicated PCB are shown in Fig. 11(a) and (b), respectively. The fabricated 65nm dice along with all off-chip components of the LV side are supplied by a 2 V supply while drawing 5 mA. The HV side of the PCB is supplied by ±2.5 V and consumes 20 mW approximately. The modulated current of the miniature coil being fed by the HV side's driver is shown in Fig. 11(c), which represents the modulated magnetic field of the coil.

On the HV side, AD4940 is chosen to drive the miniature coil for sufficient driving capability and rapid response. Chopper switches on both high and low side are implemented using commercially available multiplexers "ADG511 & ADG787", and the non-overlap clocks of Fig. 4(a) are created using NANDs "CD4011 & SN74HC00" and inverters "CD4049 & SN74HC04". Proper clocking signal between modulator and demodulator switches need to be precisely regulated. Any variation of duty cycle from 50% adds to system input referred offset; frequency mismatch causes harmonic and distorts the output signal. Moreover, the unadjusted clock phase causes signal attenuation; consequently, LV side switches must have an identical delay as the signal paths to avoid signal loss. Therefore, to address these concerns, an accurate switching operation is achieved by using the Keysight 33600A arbitrary waveform generator.

The fabricated chip using TSMC 65nm is shown in Fig. 12(a). This chip has 0.6 mm length and 0.4 mm height, and

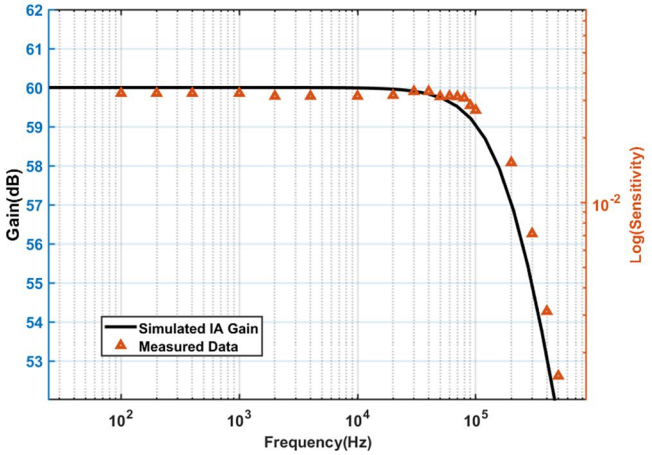

Fig. 13. Simulated frequency response of the implemented IA compared with measured frequency response of the combined integrated sensor and IA's sensitivity.

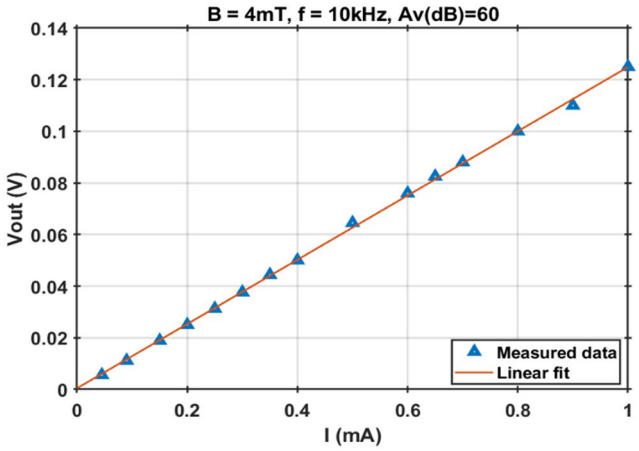

Fig. 14. Sensor output voltage for different biasing currents.

it consists of two sensors surrounded by metallic shield and corresponding IAs. The metallic shield is formed by 5 layers of hexagonal spiral coils with outer diameter of 150 µm and inner diameter of 15 µm leaving the central gap open for magnetic field entry. The initial purpose of the spiral coils was to generate a high integrated magnetic field; however, the measurement results revealed that the effect of differential capacitive coupling "$V_{diff-cc}$" explained in section II-E becomes dominant at frequencies above 50 kHz, and the amplified signal would not be purely magnetic based. Therefore, to have purely Hall effect without interference of capacitive coupling, the integrated spiral coil is used as a shield and is tied to ground, and an external miniature coil is utilized, as shown in Fig. 12(b). To double the sensitivity, the two implemented sensors are serially connected, and they generate 180-degree phase difference signals.

Distance from the on-chip miniature coil to the dice is directly and inversely proportional to RMS isolation voltage and SNR, respectively. That is, as the separation distance between the coil and die increases, magnetic field drastically attenuates. Consequently, to capture the most magnetic field, at 0.05 mm of Fig. 8, the coil is placed and glued on the chip top with a no-shrink/expand very low viscosity epoxy as depicted in Fig. 12(c).

The CMOS Hall elements have a bandwidth in the range of few megahertz [23]. To investigate the sensor and IA's bandwidth and sensitivity, a resonant technique as reported in [27] is employed. First, the DC voltage sensitivity of a single sensor at 1mA biasing current is measured using the GMW 3472 Dipole Electromagnet generating a 4 mT of magnetic field. Next, on the measurement setup of Fig. 12(c), the miniature coil is connected to a signal generator, and a DC voltage that yields the same sensitivity is defined. Finally, for the same magnitude as of DC voltage, a resonant capacitor is serried with the miniature coil, and the signal generator frequency is tuned to achieve the maximum peak (resonant frequency) and the resonant frequency is recorded. The resulted sensitivity of the sensor at different frequencies is shown in Fig. 13 and the single sensor's sensitivity of 0.032 V/mAT is bounded by the IA's bandwidth. The measured sensitivity complies with the calculated sensitivity reported in Fig. 5. Also, the sensor's output voltage that linearly varies with the biasing current is shown in Fig. 14. This confirms the purely resistive feature of the sensor. Additionally, the measured resistivity between sensor voltage nodes is 850 Ω. Accordingly, following Fig. 14, although increasing biasing current escalates sensor's sensitivity, having two sensors in series with 1 mA of current consumes 1.7 V of supply rail and sourcing more current is not applicable.

Having rapid response time in amplifiers' chain from the HV to LV side requires a sharp modulated signal before the demodulator choppers to preserve the signal amplitude. In consequence, modulation frequency must be chosen based on the slew rate and the bandwidth limit of the amplifiers' chain including the driver, sensors, and integrated IAs, as well as the input signal spectrum. Knowing the measured 200 kHz bandwidth of the combined implemented Hall-IA shown in Fig. 13, 100 kHz is chosen as the chopping frequency. The 3dB frequency of the HPF of Fig. 4 is chosen to be 20 kHz to sufficiently attenuate the PGA "LTC6910" input signal from flicker noise and DC offset. The relatively low modulation frequency and the input signal bandwidth ranging from DC to 10 kHz obliged us to use a 4th order active low pass AAF filter which is realized in this test setup by the active filter IC "LTC1563".

The measured inductance and resistance of the manufactured coil with the ferrite rod inside are 0.25 mH and 12 Ω, accordingly. To create a wide passband frequency response on the HV side, a serried capacitance of 50 nF and a 2 kΩ resistance are included.

In this Hall based GA, the coil-dice distance defines system's isolation level, and the aggression current must pass the magnetic barriers to break the amplifier's ground loops. The magnetic wire of the coil has polyamide insulation coating with 10 µm thickness, so considering zero distance between the die with its bond wires and surface of coil-copper's enamel, as shown in Fig. 9(b), minimum continuous isolation level of 550 V is guaranteed [28]. Therefore, this design benefits from a minimum of 0.55 kV of continuous isolation working voltage "V_{iso}", which can further be improved by increasing the polyamide barrier thickness.

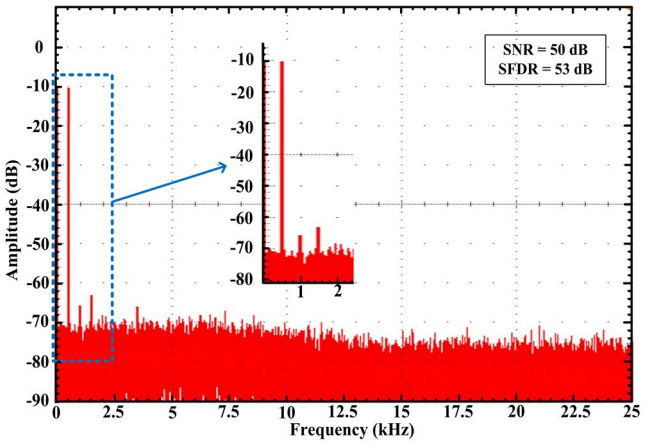

Fig. 15. Output spectrum of a ±250 mV input signal at 500 Hz.

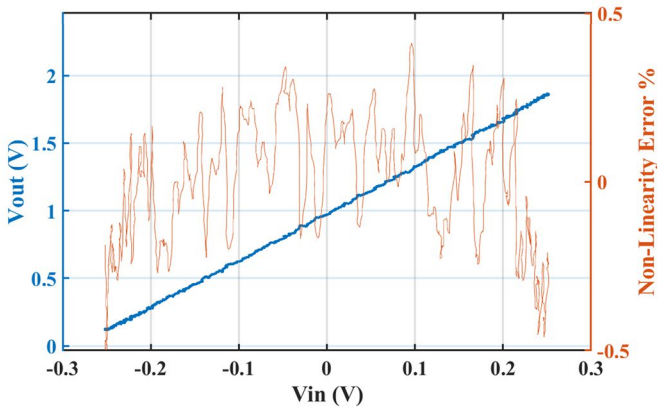

Fig. 16. Amplifier's output nonlinearity error for input differential voltage of ±0.25 V.

The overall input referred offset of the design is 1 mV. The output spectrum of the amplifier attains an overall SNR of 50 dB within the 10 kHz bandwidth and an SFDR of 53 dB as shown in Fig. 15. It can be seen from the spectrum graph that the modulation/demodulation approach has eliminated the 1/f noise from the output spectrum and based on 6 kV/V gain from Hall element to the output, the -72 dB of noise spectrum in signal band corresponds to amplified thermal's noise of the combined sensors and amplifiers.

The gain error for the output voltage swing of 0.1 to 1.9 V is shown in Fig. 16 yielding a maximum nonlinearity error of 0.5%. In this measurement, employing least squares between differential input voltage (V_{in+} - V_{in-}) and differential output voltage (V_{out+} - V_{out-}), slope of the optimum line is defined. Then, nonlinearity is calculated as a fraction of half of the peak-to-peak value of differential output voltage deviation divided by the full-scale differential output voltage range. The measured amplifier's 5 µs propagation delay time in response to input step function is shown in Fig. 17, which is sufficient for any over current conditions [3].

Table III summarizes the performance and the comparison with the state-of-the-art and industrial isolated amplifiers. Unlike conventional Hall sensor, high input impedance of the drivers shaped the design to be capable of voltage and current sensing through shunt resistors. In this implementation, a dedicated external supply for the high side is required; thereafter, in comparison with the same category of amplifier

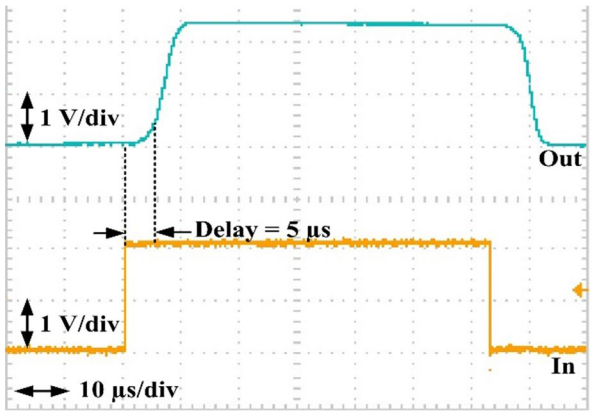

Fig. 17. Step Response and Propagation Delay time.

TABLE III
PERFORMANCE SUMMARY AND COMPARISON WITH PRIOR -ART WORKS

Parameter	[3]	TLP7920 [4]	HLSR 50 [18]	This Work
Isolation Type	Inductive	Optic	Hall Effect	Hall Effect
Data Transmission	Digital	Digital	Analog	Analog
Sensing Application	Voltage/ Current	Voltage/ Current	Current	Voltage/ Current
V_{iso} [kV]	0.6	0.6	4.3	0.55<
Power [mW]	251.5	60 (HV side)/ 18.6 (LV side)	95	20 (HV side)/ 10 (LV side)
Input range	±0.3 V	±0.2 V	±125 A	±0.25-2.5 V
Vout non-linearity % @ minimum input range	0.5%	0.02%	0.5%	0.5%
Bandwidth [kHz]	200	230	400	10
Input offset	0.7 [mV]	0.73 [mV]	313 [mA]	1 [mV]
SNR [dB] @ bandwidth	71.9	-	59.1	50
SFDR [dB]	84.6	-	-	53
Propagation delay [µs]	5	2.8	-	5

(e.g. TLP7920 [4]), the Hall based GA has significantly conserved total consumption due to the elimination of the HV side's ADCs. Finally, the minimum V_{iso} of 550 V is insured and by benefitting from polyamide layer of commercially available technologies including 0.18 µm or adding 30 to 50 µm of polyamide layers by an external process, RMS isolation voltage can be further improved while losing about 0.5 dB of SNR as shown in Fig. 8. Also, manufacturing coils with a smaller inner diameter and using thinner wires reduce its outer diameter such that the chip diameter is larger than the coil. Thereafter, the process of attaching the coil to the chip becomes easier and more adaptable to pick and place equipment.

IV. CONCLUSION

To the authors' best knowledge, the reported work is a preliminary proof of concept of a novel approach in using Hall sensors as isolation amplifiers. A System in Package solution for analog isolation amplifier based on CMOS integrated Hall sensor is presented for voltage and shunt resistor current sensing, while satisfying minimum RMS isolation working

voltage of 550 V. The isolated amplifier yields an input offset of 1 mV, overall SNR of 50dB with 10 kHz bandwidth, SFDR of 53dB, and 5 µs propagation delay.

The author is currently working on improvement of the design. Using miniature coils with 10µm of wire diameter or special packaging having integrated coils can further improve the system's overall SNR and compactness. In application where higher SNR is required, 2DEG sensors, namely GaN, can be utilized. Sensor's sensitivity drift over temperature needs to be compensated, and all the off-chip components including PGA and filter can be integrated. Finally, for a complete isolation amplifier, a clock recovery with a tunable phase as well as an isolated power converter is needed.

ACKNOWLEDGMENT

The authors would like to acknowledge the financial support from Natural Sciences and Engineering Research Council of Canada (NSERC), and the design and simulation tools supported by CMC Microsystems.

REFERENCES

[1] "IEC 61800-5-2", "Adjustable speed electrical power drive systems - Part 5-2: Safety requirements - Functional", 2016.

[2] Texas Instrument, "AMC1301 Precision, ±250-mV Input, 3-µs Delay, Reinforced Isolated Amplifier". [Online]. Available: http://www.ti.com. Accessed: Apr. 2020.

[3] S. Ma, J. Feng, T. Zhao, and B. Chen, "A Fully Isolated Amplifier Based on Charge-Balanced SAR Converters," IEEE Transactions on Circuits and Systems I: Regular Papers, vol. 65, no. 6, pp. 1795-1804, 2018, doi: 10.1109/TCSI.2017.2767678.

[4] "Photocouplers Optically Isolation Amplifier, TLP7920,TLP7920F", TOSHIBA. [Online]. Available: https://toshiba.semicon-storage.com/. Accessed: Sep. 2020.

[5] C. A. McCreary and B. A. Lail, "Design of multiple stage avionics lightning protection for DC power input lines using a graphical user interface (GUI)," in 2013 IEEE International Symposium on Electromagnetic Compatibility, Aug. 2013, pp. 177-181, doi: 10.1109/ISEMC.2013.6670404.

[6] "ISO124: ±10-V Input, Precision Isolation Amplifier", Burr-Brown Products from Texas Instruments. [Online]. Available: http://www.ti.com. Accessed: June 2018.

[7] A. Devices. "AD215: 120 kHz bandwidth low distortion isolation amplifier". [Online]. Available: http://www.analog.com. Accessed: Sep. 2019.

[8] F. Rothan et al., "A ±1.5% nonlinearity 0.1-to-100A shunt current sensor based on a 6kV isolated micro-transformer for electrical vehicles and home automation," in 2011 IEEE International Solid-State Circuits Conference, Feb. 2011, pp. 112-114, doi: 10.1109/ISSCC.2011.5746242.

[9] S. Takaya, H. Ishihara, and K. Onizuka, "18.7 A DC to 35MHz Fully Integrated Single-Power-Supply Isolation Amplifier for Current- and Voltage-Sensing Front-Ends of Power Electronics," in 2020 IEEE International Solid- State Circuits Conference - (ISSCC), Feb. 2020, pp. 298-300, doi: 10.1109/ISSCC19947.2020.9063124.

[10] "Designing Linear Amplifiers Using the IL300 Optocoupler", Application Note 50. [Online]. Available: www.vishay.com. Accessed: Sep. 2019.

[11] "Gauging LED lifetime in optocouplers". [Online]. Available: https://www.machinedesign.com/news/gauging-led-lifetime-optocouplers. Accessed: Sep. 2019.

[12] A. H. Johnston and B. G. Rax, "Proton damage in linear and digital optocouplers," IEEE Transactions on Nuclear Science, vol. 47, no. 3, pp. 675-681, 2000, doi: 10.1109/23.856497.

[13] S. Ziegler, R. C. Woodward, H. H. Iu, and L. J. Borle, "Current Sensing Techniques: A Review," IEEE Sens. J., vol. 9, no. 4, pp. 354-376, 2009, doi: 10.1109/JSEN.2009.2013914.

[14] S. S. Mirfakhraei, Y. Audet, A. Hassan, M. Ali, M. Nabavi, and M. Sawan, "A CMOS MAGFET-Based Programmable Isolation Amplifier," in 2020 18th IEEE International New Circuits and Systems Conference (NEWCAS), June 2020, pp. 9-13, doi: 10.1109/NEWCAS49341.2020.9159790.

[15] S. S. Mirfakhraei et al., "Wide Dynamic Range Front-End Programmable Isolation Amplifier using Integrated CMOS Hall Effect Sensor," in 2020 IEEE International Symposium on Circuits and Systems (ISCAS), Oct. 2020, pp. 1-5, doi: 10.1109/ISCAS45731.2020.9180574.

[16] W.-c. Wang, "A Motor Speed Measurement System Based on Hall Sensor," in Intelligent Computing and Information Science, Berlin, Heidelberg, R. Chen, Ed., 2011// 2011: Springer Berlin Heidelberg, pp. 440-445.

[17] ALLEGRO microsystems, "ACS714, Automotive Grade, Fully Integrated, Hall-Effect-Based Linear Current Sensor IC with 2.1 kVRMS Voltage Isolation and Low-Resistance Current Conductor". [Online]. Available: https://www.allegromicro.com/. Accessed: Aug. 2020.

[18] "Current Transducer HLSR-P series". [Online]. Available: http://www.lem.com. Accessed: Apr. 2018.

[19] MELEXIS. MLX91208, "IMC-Hall® Current Sensor (Triaxis®Technology)". [Online]. Available: www.melexis.com. Accessed: June 2018.

[20] BROADCOM. ACHS-719X, "Fully Integrated, Hall Effect-Based Linear Current Sensor IC with 3 kVRMS Isolation and Low-Resistance Current Conductor". [Online]. Available: www.broadcom.com. Accessed: July 2020.

[21] "Isolation Types and Considerations When Taking a Measuremen." [Online]. Available: https://www.ni.com/.

[22] A. Chovet, C. S. Roumenin, G. Dimopoulos, and N. Mathieu, "Comparison of noise properties of different magnetic-field semiconductor integrated sensors," Sensors and Actuators A: Physical, vol. 22, no. 1, pp. 790-794, 1990/06/01/ 1990, doi: https://doi.org/10.1016/0924-4247(89)80079-2.

[23] Y. Xu and H.-B. Pan, "An improved equivalent simulation model for CMOS integrated Hall plates," (in eng), Sensors (Basel), vol. 11, no. 6, pp. 6284-6296, June 2011, doi: 10.3390/s110606284.

[24] Y. Xu, H.-B. Pan, S.-Z. He, and L. Li, "A Highly Sensitive CMOS Digital Hall Sensor for Low Magnetic Field Applications," Sensors (Basel), vol. 12, pp. 2162-74, Dec. 2012, doi: 10.3390/s120202162.

[25] M. Demierre, S. Pesenti, J. Frounchi, P.-A. Besse, and R. Popovic, Reference Magnetic Actuator for self Calibration of a very small Hall Sensor Array. Apr. 2002, pp. 39-46.

[26] M. M. Marco Crescentini, Aldo Romani, Marco Tartagni, Pier Andrea Traverso, "Bandwidth limits in Hall effect-based current sensors," vol. 6, no. 4, pp. 17-24, Dec. 2017.

[27] High-Frequency Electromagnet Using Resonant Technique. [Online]. Available: https://www.accelinstruments.com/Applications/WaveformAmp/Electromagnetic-Coil-Resonant.html. Accessed: Sep. 2020.

[28] CnC Tech Industrial Cable and Connector Technology, "MW35C". [Online]. Available: https://www.cnctech.us/pdfs/MW-Specification-sheet.pdf. Accessed: Sep. 2020.

Seyed Sepehr Mirfakhraei received his M.Eng degree in signal processing and communication from Boston University, MA, USA in 2014. He is working as Ph.D. student in Polystim Neurotechnologies laboratory at Ecole Polytechnique de Montreal, Montreal, QC, CANADA from 2018. Sepehr's research aim is design and development of programmable isolation amplifier based on Hall effect sensors.

Yves Audet (M' 01) received his B.Sc. degree and M.Sc. degree in physics from the University of Sherbrooke, Quebec, Canada in 1989 and 1992, respectively. He also obtained a DEA diploma from University Joseph Fourier in Grenoble, France in 1990. He completed his Ph.D. at Simon Fraser University, BC, Canada in 1996 working on large integrated sensor arrays.

He was with the Research and Development group at Mitel Semiconductor, Kanata, Ontario, Canada from 1996 to 1999 where he was involved in the design and characterization of mixed signal CMOS circuits. Since 2001, he is Professor in the Department of Electrical Engineering at Polytechnique of Montreal, Quebec, Canada. His research interests are CMOS sensors, imaging sensors, fault tolerant circuit architecture for avionics, and energy harvesting.

Ahmad Hassan received the Ph.D. degree in electrical engineering from Polytechnique Montreal, QC, Canada, in 2019. He is currently a postdoc in Polystim Neurotechnologies laboratory at Ecole Polytechnique de Montreal, Montreal, QC, Canada. Ahmad's research is oriented towards high temperature microelectronics, including design and implementation of wireless power and data transmission systems dedicated for harsh environment applications.

Mohamad Sawan (S'88-M'89-SM'96-F'04) received the Ph.D. degree in 1990 in Electrical Engineering, from Sherbrooke University, Canada. He is a Chair Professor Founder and Director of the Center for Biomedical Research And INnovation (CenBRAIN) in Westlake University, Hangzhou, China. He is Emeritus Professor of Microelectronics and Biomedical Engineering and he is founder and director of the Polystim Neurotech Laboratory in Polytechnique Montréal. He was leading the Microsystems Strategic Alliance of Quebec (1991-2019). Dr. Sawan is Vice-President Publications (2019-Present) of the IEEE CAS Society, he is founder of the interregional IEEE NEWCAS conference, co-founder and Editor-in-Chief of the IEEE Transactions on Biomedical Circuits and systems (2016-2019). He supervised the thesis of more than 120 Master and 60 Ph.D. students. He published more than 800 peer reviewed papers, was awarded 12 patents, and 11 other patents are pending. Dr. Sawan received several awards, among them the Queen Elizabeth II Golden Jubilee Medal, the Shanghai International Collaboration Award, the Bombardier Award for technology transfer, the Jacques-Rousseau Award, the medal of merit from the President of Lebanon, and the Barbara Turnbull Award for spinal cord research in Canada. He is Fellow of the IEEE, Fellow of the Canadian Academy of Engineering, Fellow of the Engineering Institute of Canada, and Officer of the Quebec's National Order.